

Three-dimensional direct laser writing of biomimetic neuron interfaces in the era of artificial intelligence: principles, materials, and applications

Haoyi Yu,^{a,b} Qiming Zhang^{✉,a,b} Xi Chen,^{a,b} Haitao Luan,^{a,b} and Min Gu^{a,b,*}

^aUniversity of Shanghai for Science and Technology, Institute of Photonic Chips, Shanghai, China

^bUniversity of Shanghai for Science and Technology, School of Optical-Electrical and Computer Engineering, Centre for Artificial-Intelligence Nanophotonics, Shanghai, China

Abstract. The creation of biomimetic neuron interfaces (BNIs) has become imperative for different research fields from neural science to artificial intelligence. BNIs are two-dimensional or three-dimensional (3D) artificial interfaces mimicking the geometrical and functional characteristics of biological neural networks to rebuild, understand, and improve neuronal functions. The study of BNI holds the key for curing neuron disorder diseases and creating innovative artificial neural networks (ANNs). To achieve these goals, 3D direct laser writing (DLW) has proven to be a powerful method for BNI with complex geometries. However, the need for scaled-up, high speed fabrication of BNI demands the integration of DLW techniques with ANNs. ANNs, computing algorithms inspired by biological neurons, have shown their unprecedented ability to improve efficiency in data processing. The integration of ANNs and DLW techniques promises an innovative pathway for efficient fabrication of large-scale BNI and can also inspire the design and optimization of novel BNI for ANNs. This perspective reviews advances in DLW of BNI and discusses the role of ANNs in the design and fabrication of BNI.

Keywords: direct laser writing; neuron interface; neural tissue engineering; artificial neural networks.

Received Jan. 13, 2022; revised manuscript received Mar. 2, 2022; accepted for publication May 3, 2022; published online Jun. 7, 2022.

© The Authors. Published by SPIE and CLP under a Creative Commons Attribution 4.0 International License. Distribution or reproduction of this work in whole or in part requires full attribution of the original publication, including its DOI.

[DOI: [10.1117/1.AP.4.3.034002](https://doi.org/10.1117/1.AP.4.3.034002)]

1 Introduction

Over the past two decades, the research interest in neuron science and artificial intelligence (AI) has increased dramatically,^{1–3} as progress in neuron science is expected to lead to a higher level of understanding the brain, and eventually the creation of smarter artificial neural networks (ANNs).^{4,5} This co-dependence of technology and scientific research in biology will inevitably end with the merging of natural and artificial systems. However, such an endeavor remains a formidable task, as our current state of engineering does not allow for seamless integration of those two naturally dissimilar systems. Toward this aim, biomimicry⁶ is regarded as an innovative solution in biofabrication and

biological applications, introducing models and designs from nature.^{7–9} Plenty of collaborative brain projects have been proposed around the globe, including the Brain Initiative,¹⁰ the Human Brain Project,^{11,12} China Brain Project,¹³ Brain Mapping by Integrated Neurotechnologies for Disease Studies,¹⁴ and the Brain Alliance.¹⁵ These projects have stimulated an intense research field to create various two-dimensional (2D) and three-dimensional (3D) biomimetic neuron interfaces (BNIs),^{16–19} where biological neuron tissues could be integrated into an artificial extracellular matrix^{20–22} to rebuild, understand,^{23–26} and improve neuronal functions in neuron tissue engineering,^{21,27–30} and also enable physicists to achieve novel BNIs toward the development of ANNs.^{6,31,32}

However, these BNI approaches remain outmatched by biological neural networks (BNNs). The BNNs are well known to

*Address all correspondence to Min Gu, gumin@usst.edu.cn

be complex 3D structures with organized neuron connections from millimeter to nanometer scales,^{33,34} while neurons engineered on a 2D interface by 2D lithography grow typically in a monolayer fashion,³⁵ and could not replicate the 3D feature in BNNs. A 3D large-scale printed BNI by 3D additive printing could not guide the growth of neurons at a single neuron scale or below,³⁶ therefore limiting its capability of creating 3D BNI with micrometer- or nanometer-scale resolution.

Due to these reasons, the use of 3D direct laser writing (DLW), a single-step, mask-free, and nanoscale/microscale fabrication technique,³⁷ has witnessed an explosive increase in creating BNIs. Compared with traditional advanced manufacturing techniques, such as 2D electron beam lithography and 3D additive printing, the technology enables the realization of arbitrary 2D and 3D structures at the nanometer to micrometer scale, where the smallest feature size can be 9 nm via the use of super-resolution photoinitiation–inhibition nanolithography (SPIN)-based laser fabrication.³⁸ However, the current DLW of BNI faces significant inefficiency in the scale-up of the BNIs.³⁹

ANNs,⁴⁰ which are computing algorithms inspired by the BNNs based on a collection of connected units or nodes named “artificial neurons,” have shown their unprecedented ability to improve efficiency in applications such as data processing and image recognition/classification.^{41–43} The integration of ANNs in the DLW system could provide new approaches toward higher complexity, higher connectivity in BNIs, as well as the discovery and design of BNIs for ANNs.

In this perspective, we review the recent development of DLW of BNIs and explore the future prospect of ANNs in DLW. The development of BNIs is discussed first, where we examine the milestone developments in BNIs, emphasizing the necessity of achieving the 3D scale-up of BNIs. Then, we detail the principles, materials, and applications of DLW technology in BNIs. Finally, we address future research possibilities and challenges in the field, stressing that the integration of DLW technology and ANNs are critical for the next generation of 3D BNIs.

2 Toward Building Biomimetic Neuron Interfaces with Nanoscale Resolution in 3D

The development of BNIs has witnessed ongoing technological innovations toward achieving more complex biomimetic neuron structures (Fig. 1): from 2D to 3D.⁴⁵ Different lithographic and bio-printing techniques have been utilized to create microstructures using biologically compatible materials. Primitive designs of biomimetic neuron structures are based on 2D through-holes,³⁵ microtunnels,⁴⁶ microtroughs,⁴⁷ and microwells⁴⁸ on biocompatible materials, such as polydimethylsiloxane parylene and hydrogels. Recent developments of the 3D additive printing technique have also demonstrated its potential in building large-scale 3D BNIs.⁴⁹ These neuron interfaces have been very effective for studying neuron activities,^{50,51} and also a platform to

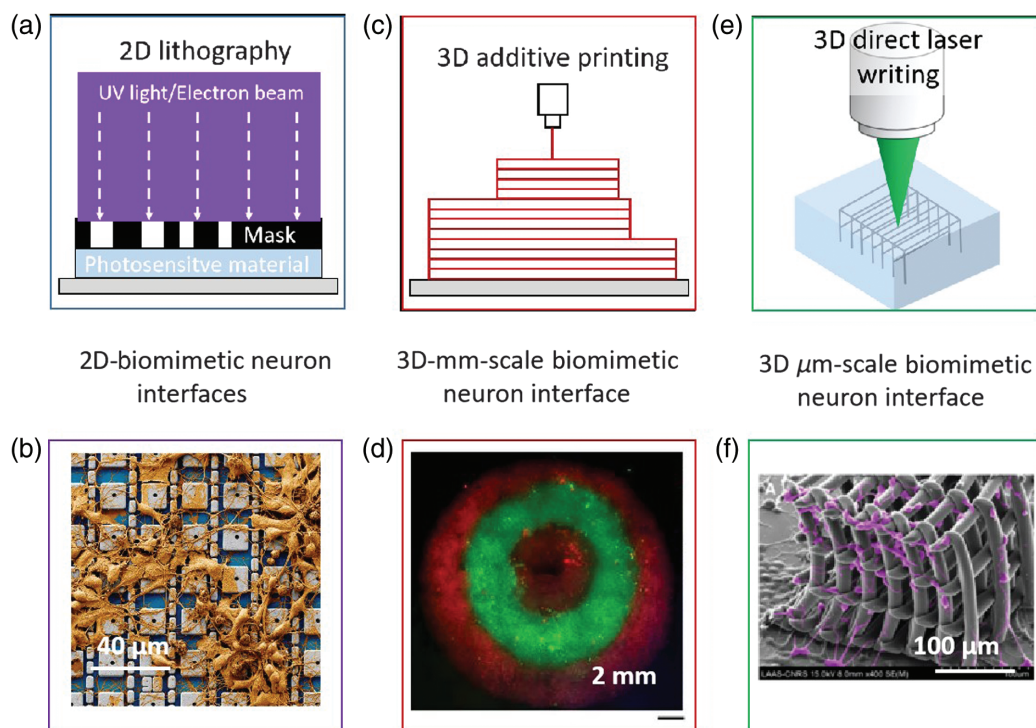


Fig. 1 Recent developments of building BNIs at different scales. (a) and (b) Schematic of 2D lithography of BNIs; 2D BNIs fabricated on a CMOS nanoelectrode array improved the nanobio interface to enable intracellular recording from rat neurons. The device contains a $64 \times 64 = 4096$ nanoelectrodes, array and records intracellular signals from more than 1700 rat neurons;¹⁷ (c) and (d) schematic of 3D additive printing of BNIs; 3D additive printing of bioengineered 3D brain-like layered structures;²⁰ and (e) and (f) schematic of 3D DLW of BNIs; DLW of 3D BNI in hydrogel material.⁴⁴

Table 1 Different approaches employed toward the realization of BNIs and key achievements in each field.

| Technique | Key achievements | References |
|-----------------|---|----------------|
| 2D lithography | CMOS nanoelectrodes array enabling the intracellular recording from rat neurons | 17 |
| | Modulation of neural network activity by 2D patterning | 35 |
| | Neuron synaptic connectivity | 57 |
| | Learning process in networks of cortical neurons | 53 |
| | Reliable neuronal logic devices | 54 |
| 3D bio-printing | Brain like structure for primary cell proliferation and network formation | 20 |
| | <i>In vivo</i> and controllable dual-drug release behaviors | 55 |
| 3D DLW | 3D real-time neuron migration | 58 |
| | 3D neurite/neuron network orientation and formation | 59 and 60 |
| | 3D network-like structure for neuron force measurement | 61 |
| | 3D neuron network growth guidance | 50, 62, and 63 |
| | 3D waveguides connection for CNNs computing | 64 |

realize neuron computing.⁵² Traditional studies in BNIs generally focus on utilizing the BNIs to assist in the passive study of *in-vivo* neuronal functions, such as intracellular neuron signals study,¹⁷ neuron synaptic study,⁵³ modulation of 2D neuron activities,⁵⁴ construction of neuronal logic devices,⁵⁵ and drug release study.⁵⁶ The key achievements and approaches are summarized in Table 1.

However, the current 2D methods cannot achieve the 3D spatial extensions of neuron axons and dendrites, with the largest number of neurons around 1700, still far behind the neuron

numbers in animal brains [see Figs. 1(a) and 1(b)].¹⁷ In addition, 3D additive printing is able to achieve millimeter-scale neuron interfaces but the fabrication resolution limits its capability of creating 3D BNI with micrometer- or nanometer-scale resolution [see Figs. 1(c) and 1(d)].⁶⁵⁻⁶⁷ One potential solution toward the building of 3D and nanometer-scale BNI lies in the recent development of 3D DLW. A 3D DLW, such as single-beam two-photon DLW and two-beam SPIN, has been widely utilized to produce 3D micro/nanostructures in nanophotonics,⁶⁸ microfluidics, and biomedical implants.⁶⁹

3 Principle of 3D DLW

The fundamental phenomenon behind 3D DLW is multi-photon absorption. In this review, we shall concentrate on the theory of two-photon absorption (TPA), which can be extrapolated to three or more photons. In a 3D DLW process [see Fig. 2(a)], the photoinitiator (PI) in the photoresist absorbs two-photon energy from the focused laser beam, generating active species (radicals/ R^*) in the 3D voxel. Hence, when the density of the photo-generated active species is above a threshold, the monomers (M) in the photoresist become longer polymeric chains, resulting in a phase change (irreversible, e.g., from liquid to solid, or from one phase to another) in the central position of the 3D voxel. While in the focal volume, when the illuminated energy dose is below the threshold (surrounding area of the focal region), the concentration of the generated active species is below the required threshold for complete polymerization. This incomplete polymerization in this area will be removed later during the developing process (bath in solvents, such as isopropanol). Thus, 3D microstructures can be achieved.

The absorption efficiency of photons in the TPA process relies on the square of the illuminated light intensity. This non-linear absorption of photons results in a smaller feature size narrower than the full width at half-maximum (FWHM) by a magnitude of $\sqrt{2}$.^{56,70}

$$\text{line width (nm)} = \frac{\lambda}{2\sqrt{2}\text{NA}} \tag{1}$$

For every photoresist, the polymerization threshold is a fixed value. Therefore, by decreasing the illuminated intensity of the laser beam slowly until its intensity is higher than the

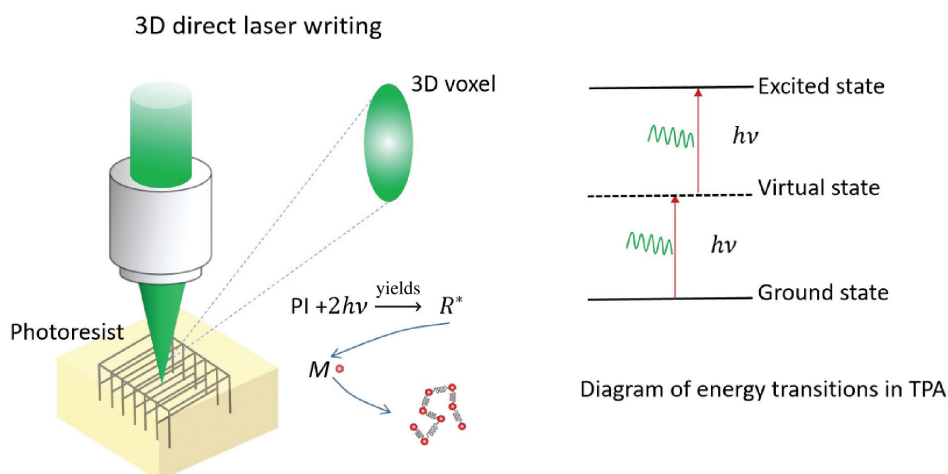


Fig. 2 Simplified diagram showing the process of 3D DLW and the TPA phenomenon.

polymerization threshold, the smallest feature size can be obtained, smaller than the diffraction limit compared with single-photon polymerization.

For 3D DLW of microstructures, the line width or feature size and the writing resolution/two-line resolution are the two characteristic parameters, which will determine the dimension and feature size of the microstructures. There are several important factors in a 3D DLW system influencing the line width and the writing resolution:⁷¹ (1) the laser source, motion system; (2) equipped optics; and (3) the photoresist or photosensitive material.

3.1 Laser Sources in 3D DLW

For the laser sources used in 3D DLW, pulsed lasers and continuous wave (CW) lasers have both been exploited in 3D DLW.⁷²⁻⁷⁴ The final characteristics of the microstructures fabricated by DLW highly rely on the excitation wavelength, the repetition rate of the laser pulse, the operation power of the laser sources, and the optics used in the systems. These performances and the qualities of the equipped optics are also critical for the feature size of the polymerization, such as the focal length and numerical aperture (NA) of the objectives. These properties will influence the energy dose delivered into the photoresist, where the polymerization mechanisms and crosslinking ratio between the polymeric chains influence the subsequent change in the

physical phase of the photoresist and the ability of the active polymeric chains to propagate and terminate between each other.^{75,76}

Until recently, femtosecond laser sources are preferred in DLW, such as the Ti:sapphire femtosecond oscillator operating at around 800 nm, and second-harmonic fiber lasers typically operating at 780 nm. A green wavelength (532 nm) amplified ultrafast yttrium aluminium garnet laser has also been used recently because they can provide a higher fabrication resolution with a smaller wavelength and low absorption in a high water content environment.⁷⁷ It has been proven to be effective in DLW under a high-water-content environment. The pulse lengths (<200 fs) and the repetition rates (50 to 80 MHz) of the laser sources in 3D DLW play significant roles in delivering the energy doses (a few nanojoules per pulse) for the polymerization process, which also relies on the photosensitivity of the material, the PI, and the focusing.

3.2 Fabrication Schemes in 3D DLW

A 3D DLW is a well-established technology for the fabrication of 3D polymer nanostructures and microstructures. In essence, the fabrication schemes of 3D DLW should be considered as an important factor as they will influence the quality of the fabrication, and for different application purposes. To use the 3D focusing voxel to write the 3D structures into the photoresist using

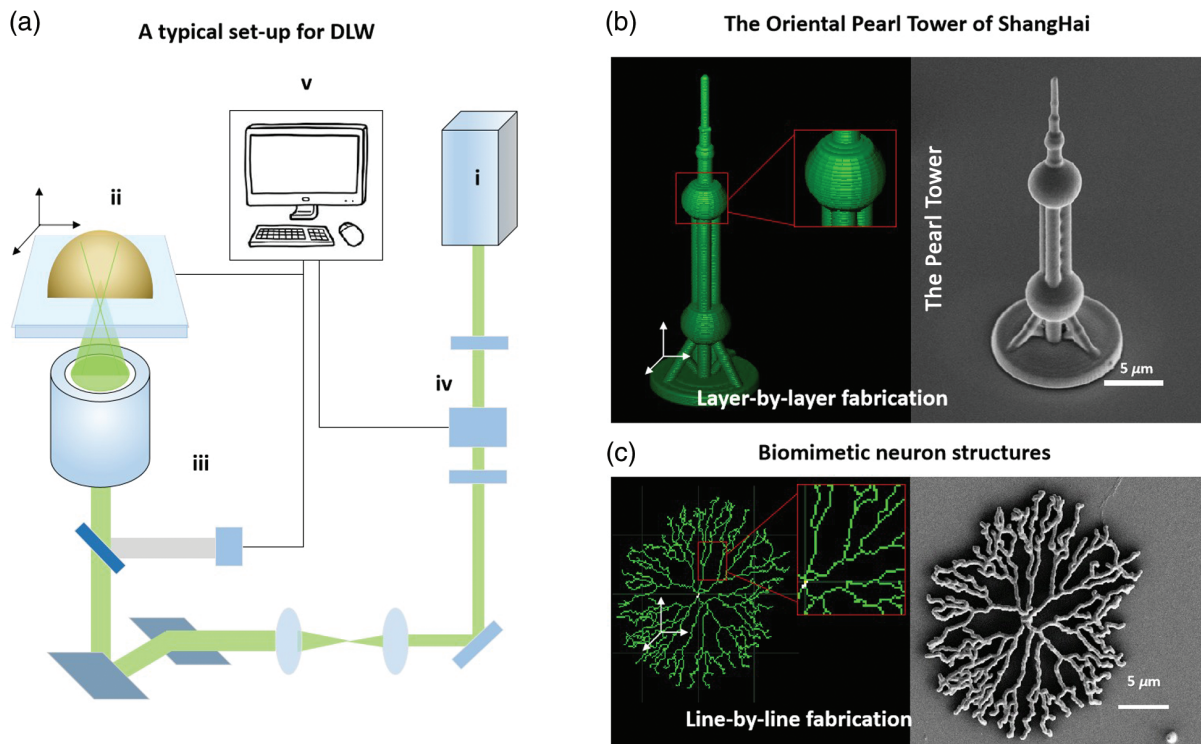


Fig. 3 (a) Schematic of a 3D DLW set-up, including (i) the laser source (ultra-fast pulsed or CW laser); (ii) a motion system consisting of nano-piezo-stages and galvo-mirrors; (iii) beam manipulation optics, which might consist of 4-*f* systems, high-NA objective, etc.; (iv) beam intensity control systems, including a shutter (either an acoustic optical modulator or a mechanical shutter); and (v) a user interface to control the system with a high-performance computer. (b) Layer-by-layer DLW fabrication of a representation of the Oriental Pearl Tower of Shanghai. Right: computer-aided design (CAD) model. Left: SEM image of the fabrication result. (c) Line-by-line fabrication of biomimetic neuron structures.⁶⁷ Right: CAD model. Left: SEM image of the fabrication result.

the focused laser beam, either the beam focus, or the sample needs to move according to the fabrication scheme that one chooses. The movement of the beam focus can be done with galvanometric scanners (galvo-mirrors), while the movement of the sample can be achieved with high-resolution x - y - z stages, as is shown in Fig. 3(a).^{78–81}

Two types of fabrication schemes are demonstrated: “the layer-by-layer fabrication” and “the line-by-line fabrication.” When using the layer-by-layer fabrication scheme, the CAD model of the target 3D microstructures is ‘sliced’ along one direction (usually along the z -direction), and each slice is separated with a slicing distance. When the “writing” of each slice is finished, a nanometric translation stage is used to move the sample along the z -direction. Using this method, the whole structure can be accomplished. This process is demonstrated in Fig. 3(b), where a 3D miniaturized “Pearl Tower of Shanghai” is fabricated using a layer-by-layer scheme in the laboratory of the Institute of Photonic Chips, the University of Shanghai for Science and Technology.

When using the line-by-line fabrication, there is no need to slice the CAD design, as fabrication can be achieved using the nanoscale stages. Due to the nm-scale accuracy of typical piezoelectric stages, the movement of the writing voxel can be as small as several nanometers, and the fabrication speed can be

hundreds of micrometers per second. For structures composed of lines, such as lattice-based photonic crystals and 3D microstructures with high porosity, a line-by-line fabrication scheme is usually used. Figure 3(c) shows a 3D biomimetic neuron being fabricated using this method.⁶⁷

Other categories of fabrication schemes are classified by whether the used objective is dipped in immersion oil or directly in the photoresists. This difference of these fabrication schemes is to compensate for the distortion resulting from the refractive index difference between the oil and the glass,⁸² which has been thoroughly discussed in a wide range of literature.

3.3 Materials Used in 3D DLW

From a technical point of view, the photoresist suitable for DLW based on TPA should consist of at least two components: a PI and a monomer. The absorption spectra of these two components should both have a transparent window at the frequency or wavelength (λ) of the operated laser. This transparency window will enable the illuminated light energy to be delivered into the volume of the photoresist without being scattered and absorbed by the bulk of the material. To achieve polymerization based on TPA, the monomer should also have a transparent window around/at the TPA wavelength ($\lambda/2$) of the PI. The success

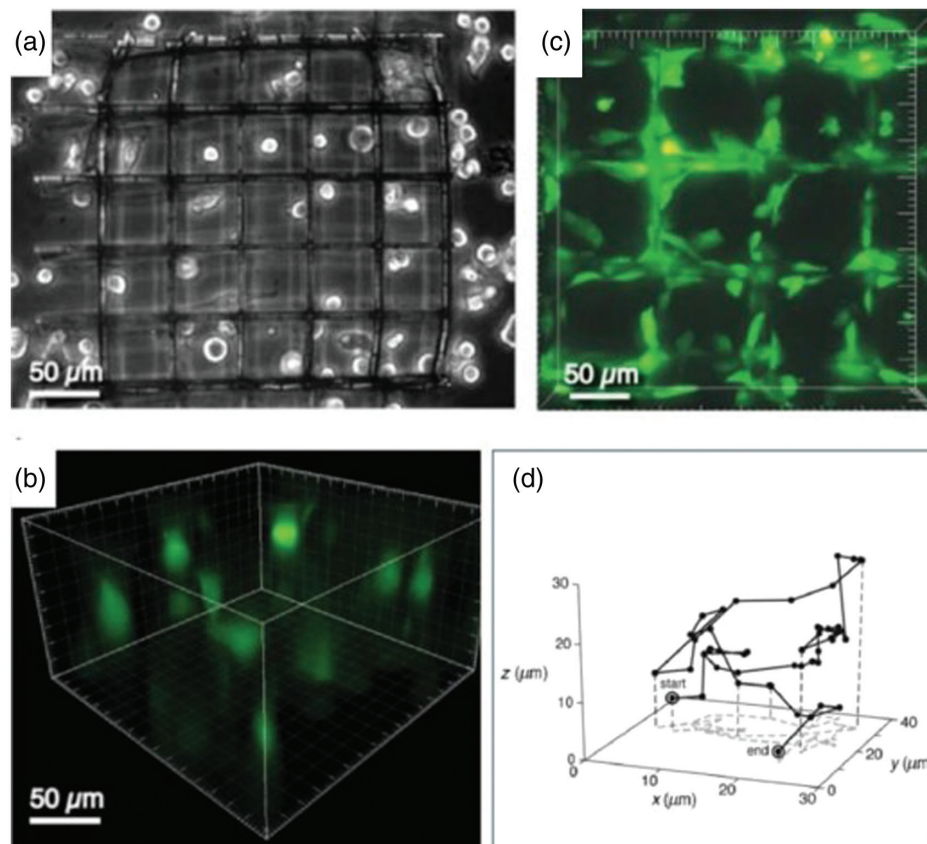


Fig. 4 The 3D BNIs for a 3D real-time neuron migration study.⁵⁸ (a) Bright-field optical microscopic image showing the distribution of cells in a 52- μm pore-sized microstructure 5 h after seeding the cells. (b) The 3D FM image showing the 3D distribution of the cells inside a scaffold 24 h after seeding the cells. (c) Top view of the fluorescent microscope of the cells in 52- μm pore-sized scaffolds showing the non-uniform distribution of the cells under varied physical obstructions. (d) Tracking of a typical cell migration phenomenon in a 25- μm scaffold.

of a proper photoresist also requires the PI to have a high two-photon cross-section,⁸³ which corresponds to a high radical quantum yield and highly active radical species generation ratio. Most of these materials are reviewed along with their applications in the following section.

4 Applications of 3D DLW of Biomimetic Neuron Interfaces

4.1 Biomimetic Neuron Interfaces for Neuron Tissue Engineering

The 3D DLW of BNIs for neuron tissue engineering application has been developed for a decade, with numerous amounts of progress toward the unveiling of the functions of the neurons.^{69,84–86} For neuron tissue engineering applications, BNIs with 3D microscale features are generally fabricated using 3D DLW. After the fabrication, biological neuron tissues would be embedded and cultured within biomimetic neuron structures. Along with the recent development in scanning electron microscopy (SEM), fluorescence microscopy, and confocal microscopy,⁸⁷ the functionalities of biological neuron cells can be studied in BNIs. Therefore, 3D DLW of BNIs has demonstrated itself as a useful tool for a wide range of neuroscience research, specifically for the investigation of neural networks in 3D *in vitro* environments, such as cell force measurement, cell migration, selective cell implants, and microfluidic applications.⁸⁸ The properties of these 3D structures by DLW, such as mechanical stiffness, geometry, biological, and chemical cues are all factors considered in the design of BNIs.

The utilization of 3D DLW to fabricate 3D microstructures was first introduced with organic materials,⁸⁹ and proved to be effective in the field of BNIs to study neuron migration,⁸⁸ as the 3D microenvironment produces higher cell migration speeds than their 2D counterparts. In these studies, organic photopolymers are used for 3D DLW, such as acrylate photopolymers.⁹⁰ This is because these materials are very easy to be synthesized and have relatively low costs, and most of these materials are transparent at visible or near-infrared wavelengths. Taylia et al. proposed using triacrylate photoresist to fabricate cage-like structures to study the migration and adhesion of the cells in 3D (Fig. 4).⁵⁸ 3D porous structures made of an acrylate photopolymer were fabricated inside the closed microchannel of a commercially available polymer chip for analysis of directed cell invasion.⁸⁴

SU-8 is a negative, epoxy-based photoresist commonly used for the fabrication of microstructures with high aspect ratios for its excellent mechanical properties, and it has been widely used in 3D DLW. SU-8 has shown its advantages in thermal stability, chemical inertness, high aspect ratio, and high cross-linking propensity, and it has been widely used to construct biomedical sensors, where the solvent-induced swelling could be minimized.^{59,91} SU-8 based microelectrodes have been fabricated to track the nerve action potential signals within the peripheral nervous system in the rat central nervous system.⁹²

Hybrid photosensitive materials have been developed for DLW due to their commercial availability and their superb properties such as high Young's modulus, optical transparency, and thermal/chemical stability,⁹³ especially because they can be fabricated with the laser at low temperatures. Three-dimensional tubular microtowers were designed and fabricated in ORMOCOMP[®] (a commercially available photoresist) to

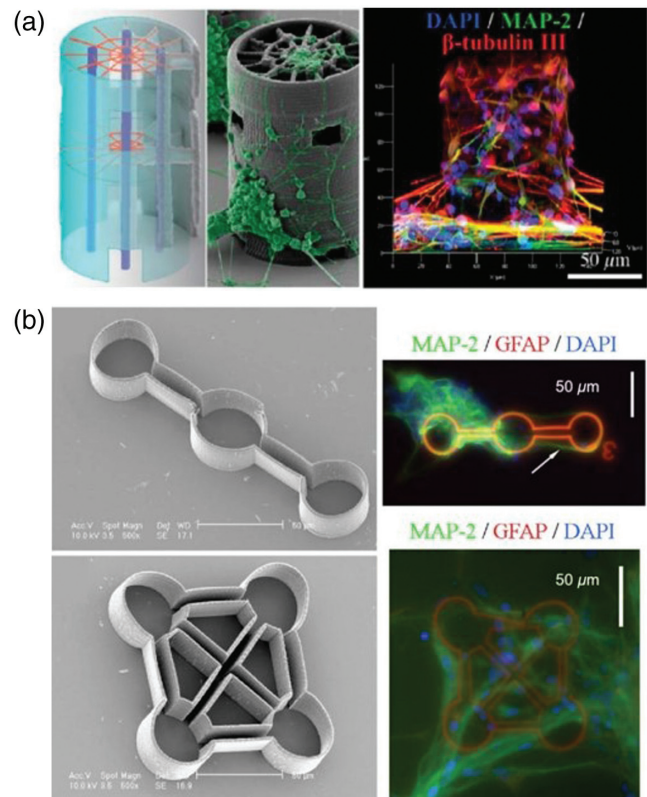


Fig. 5 3D BNIs for supporting the neurite/neuron orientation and 3D network formation. (a) Left: SEM images and the CAD model of the microtowers fabricated by 3D DLW. SEM images of neuronal cells on the microtower after one week of cell culture.⁶⁰ Right: 3D reconstruction of the confocal microscopic image showing the neuronal cell distribution on the tower. The neuronal markers are MAP-2 (green), β -tubulin III (red), and DAPI (blue). (b) Left: SEM images of neuron-cages fabricated by DLW using ORMOCER[®].⁵⁹ Right: confocal microscope images of type II and type III neuro-cages after eight days of culturing. MAP-2 (green) and astrocytes GFAP (red) are used to stain the neuronal cells.

function as neuronal cell culture platforms (see Fig. 5).⁶⁰ Due to the 3D nature of the structures, it is proved that efficient long-term 3D culturing of human neuronal cells can be achieved (the neuron cells are derived from stem cells), and these 3D structures can support the neural orientation and the neural network formation in 3D. In addition, these microtowers are designed with or without intra-luminal guidance cues and/or openings in the tower, demonstrating the strong mechanical properties of hybrid photoresists. Another most widely used photoresist is ORMOCER[®], and its variants (ORMOCOMP[®] and ORMOCLEAR[®]). This type of photoresist is commercially available⁹⁴ and has been used to fabricate microstructures to study the mobilization of the bio-tissues.⁵⁹

Other types of hybrid photoresists that have been widely used in 3D DLW are “zirconium hybrid organic-inorganic/The FORTH” photoresist,^{82,95} and SZ2080,^{96,97} both of these photoresists are optically transparent and mechanically strong.⁹⁸ These properties lead to low shrinkage, and thus make these hybrid photoresists suitable for applications sensitive to structural deformations (such as nanophotonics applications), since additional design steps are not needed to compensate for

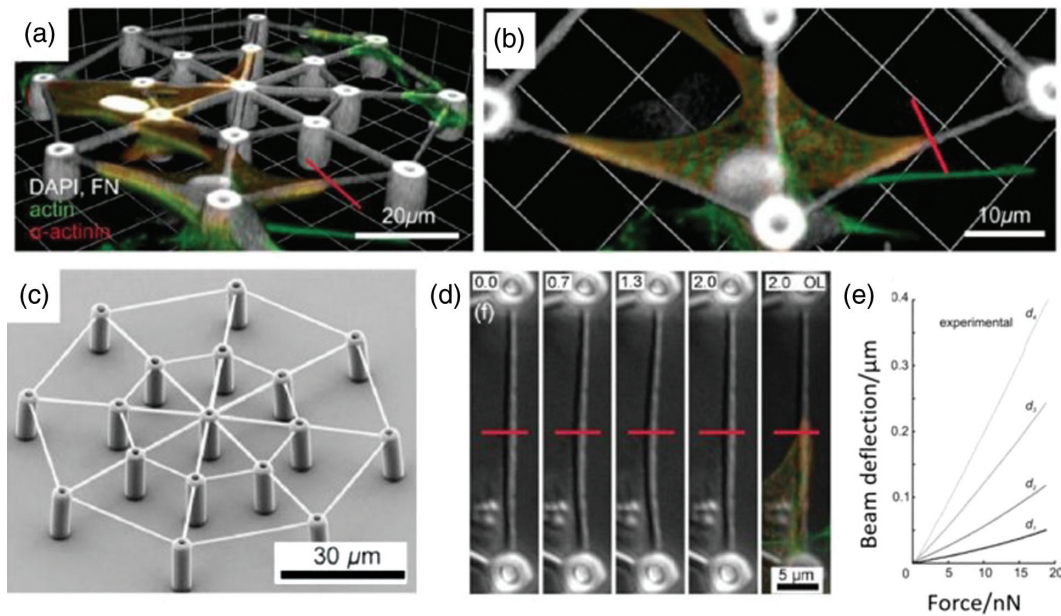


Fig. 6 Hybrid photoresist fabricated by 3D DLW of a 3D network-like structure for neuron force measurement, the photoresist is Ormocomp[®].⁶¹ (a) and (b) The 3D reconstruction of a confocal microscopic image of cardiomyocyte cells attached in the network-like microstructure, where the posts are connected by beams with a diameter of 0.6 μm (oblique view and top view). (c) The SEM image of a fully 3D network-like microstructure for cell force measurement. The sample is labeled by F-actin (green) and A-actinin (red). (d) Video frames of the deformation process of the beam in contact with the cell, where the bending of the beam can represent the cell force during one cycle of contraction (time in seconds). (e) The experimental plot of force–beam deflection, where the cell force can be calibrated by the deformation of the beams.

distortions. Its properties lead to a wide range of applications in nanophotonics and bio-tissue engineering.⁹⁹ Niches made of SZ2080 were proved to be effective to home, colonizing, and proliferating mesenchymal stem cells due to the favorable conditions provided in the microstructure.⁹⁷ 3D network-like structures were fabricated as scaffolds using ORMOCOMP for cardiomyocyte contraction force measurements (see Fig. 6).⁶¹ Cell force at the nanonewton scale can be measured by calibrating the shape deformation of the beams in the network.

Chemically modified natural polymers, such as polylactide-based (PLA) materials, have been fabricated by DLW multiphoton polymerization for neural tissue engineering scaffolds. Typically, submicrometer structures can be produced in PLA and hyaluronic acid (HA) photoresist by DLW using a femtosecond Ti:sapphire laser to promote the neuron growth guidance [see Figs. 7(a) and 7(b)].^{50,62} Photopolymerized thin-film PLA substrates and 3D microstructures were fabricated, and cell culture results showed that the photocured PLA maintained a relatively high Schwann cell purity (99%). The microenvironment also enabled cell proliferation over the length of seven days. In addition, the substrate supports Schwann cells to adhere to different directions where bi-polar and tri-polar morphologies were observed [see Fig. 7(c)].⁶³ The PLA material is suitable for applications in fabricating neural scaffolds in nerve repair.¹⁰⁰

Biodegradable hydrogel (HA) materials,^{101–104} have also attracted huge amounts of attention during recent years in biomedical research, such as functional biosensors, bio-compatible wearable devices, and self-healing materials.^{105–107} Due to their water absorbent property, high flexibility in shape deformation,

and non-toxicity, especially in the recent development of fabricating hydrogel microstructures using 3D DLW, polyethylene glycol (PEG)¹⁰⁸ is a cost-effective and Food and Drug Administration (FDA) approved synthetic hydrogel. PEG is also very compatible with a lot of different formulations for 2D and 3D additive printing. It was recently found that the crosslinking by 3D DLW of PEG-based materials, which can be cleaved and erased in water (without the need for acidic or basic additives), hold the potential for the facile modification and backbone degradation of polyether-containing materials in general. Polyethylene glycol diacrylate (PEGda) is a variant of PEG, and it can be synthesized or is commercially available.¹⁰⁹ Both PEG and PEGda have been widely used in fabricating 3D microstructures in neuron tissue engineering for their high biocomparability and versatility in adapting to various types of PIs.¹¹⁰ The crosslinked protein inside a hydrogel has been studied as scaffolds for neural cell guidance, and it was proven that complex 3D architectures can enhance the cell culture efficiency and guidance through both chemical and topographical cues, providing an effective pathway toward cell relocation and migration at micrometer scales for *in vivo* environments [see Fig. 7(b)].⁶²

Other hydrogel materials such as fibrogen and fibronectin, collagen, and bovine serum albumin (BSA) have been utilized in DLW for neuron tissue engineering. These materials are either natural polymers or proteins.^{111–113} As natural polymers and proteins, they have proven their biocompatibility in neuron tissue engineering. A live *Caenorhabditis elegans* worm was encapsulated in polymerized BSA as an *in-vivo* platform to

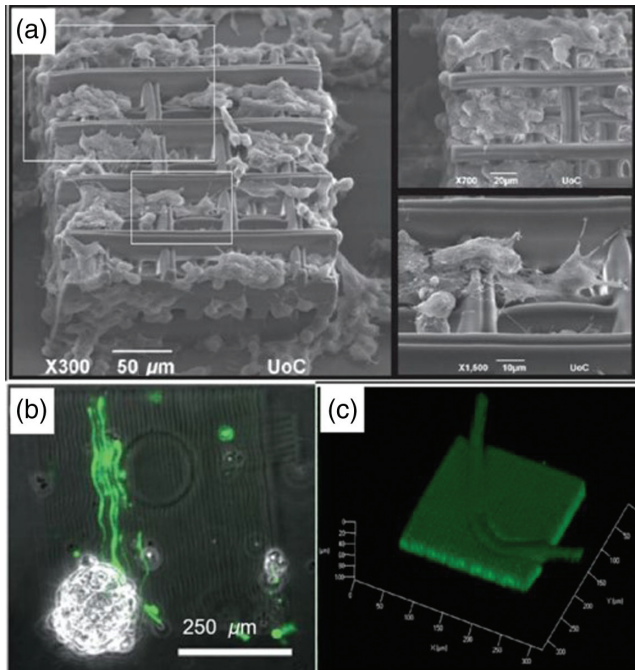


Fig. 7 Modified and natural polymers fabricated by 3D DLW for 3D neuron network guidance. (a) Microstructures fabricated using PLA to support PC12 neuronal cell growth. After five days of culturing, PC12 cells proliferate in woodpile structures (300 \times , 700 \times , and 1500 \times magnifications are shown).⁵⁰ (b) Microstructures fabricated on an HA hydrogel surface to promote the guidance growth of hippocampal progenitors (E16).⁶² Fluorescence image of the neuronal marker b-III tubulin (green) after fixation. Scale bar, 250 μm . (c) A live *C. elegans* worm encapsulated in a BSA structure on a photopolymerized microstructure (base).⁶³

study the nerve function in real-time [see Fig. 7(c)].⁶³ It is proved in this work that neuron signal transmission can be detected through microelectrodes based on BSA microstructures. The mixture of BSA and modified gelatin was also studied to create well-defined DLW scaffolds.¹¹⁴

4.2 Biomimetic Neuron Interfaces for Artificial Neural Networks

Recent development in 3D DLW of BNIs has also witnessed several advances in ANNs, as DLW enables the 3D fabrication capability at the micro/nanoscale. This fits perfectly into the desire for a parallel and energy-efficient interconnect in neuron-inspired computing.¹¹⁵ By resembling the natural counterpart (BNNs), fully or densely connected layers are the desired principal topology in ANNs, which enables massively parallel processing. A fractal topology for fully connected layers was designed and fabricated [shown in Fig. 8(a)] using 3D DLW.⁶⁴ These well-designed 3D connected waveguides functioned as convoluting optical interconnects in convolutional neural networks (CNNs). However, the low connection density (3 \times 3 artificial neuron connection array) and the high crosstalk between the waveguides remain a challenging task in this field, with several potential progresses in DLW to reduce the loss in 3D waveguides fabricated by DLW.¹¹⁷

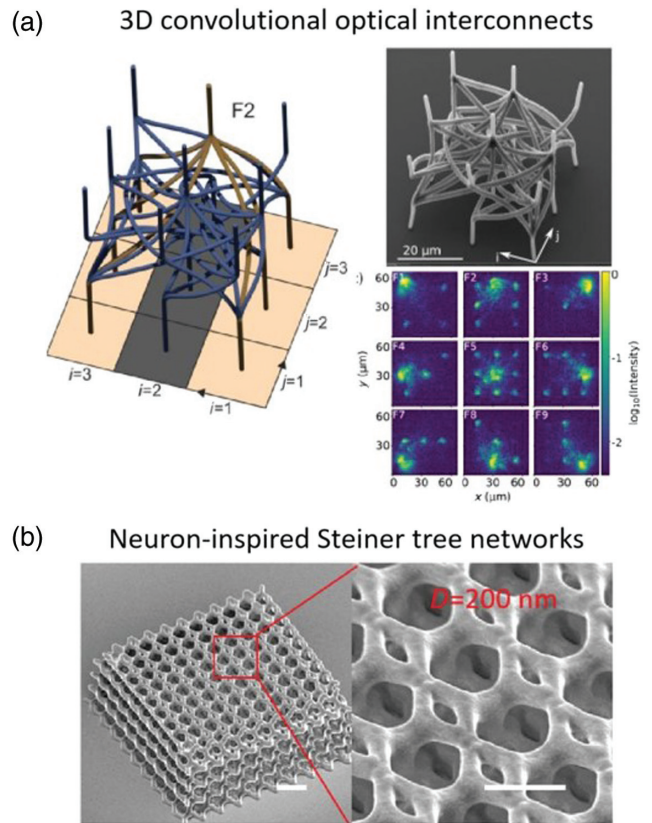


Fig. 8 BNIs for ANNs. (a) The 3D optical interconnects fabricated by 3D DLW.⁶⁴ The interconnected structure functions as a Haar filter, which is regarded as a fundamental unit in CNNs. (b) Neuron-inspired Steiner tree low-density metastructures; the scale bar is 2 μm .¹¹⁶

BNIs also have been demonstrated to be a family of low-density metastructures fabricated by 3D DLW [see Fig. 8(b)].¹¹⁶ This type of metastructure resembles the shortest connection distance in BNNs, and functions as a unique low-density meta-material hosting triple degeneracy Dirac-like points. It is also envisioned that Steiner tree metastructures might be a platform to realize zero-index material and photonic neural networks for their high degree of connectivity. Neuron-inspired nanopores that resemble the ion channels in neuron membranes have been fabricated,¹¹⁸ which might facilitate the application of artificial membranes in biological applications.

5 ANNs Enabled Efficient DLW for Large-Scale Biomimetic Neuron Interfaces

As discussed above, the DLW of BNIs has been developed for almost a decade, with various geometrical designs and materials developed and utilized for neural tissue engineering and functional ANNs applications. The future development of BNIs requires an efficient DLW system to achieve large-scale fabrication, where a large amount of data in the DLW needs to be processed efficiently.^{119,120} To satisfy this aim, developing an ANNs-enabled DLW system is the most interesting and challenging field. This section examines emerging ANNs technologies that will play an important role in the future progress in DLW of large BNIs.

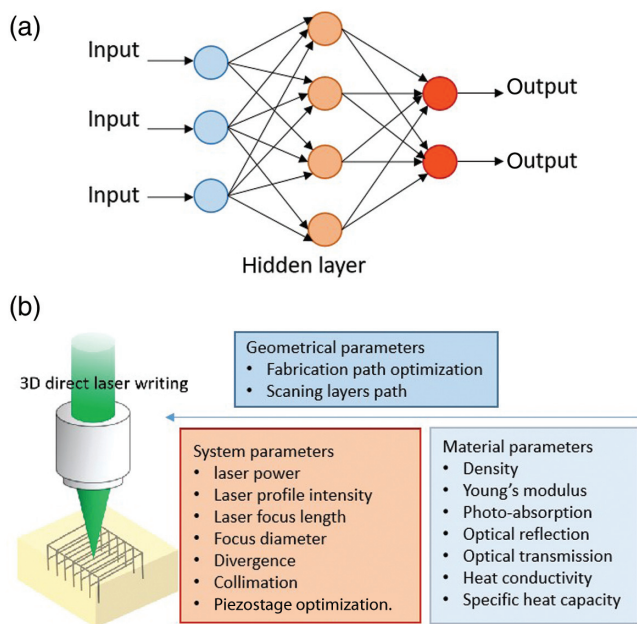


Fig. 9 (a) The structure of feed-forward ANNs. (b) The effective parameters in the 3D DLW process.

ANNs have attracted considerable attention as an advanced method to solve complex practical problems in different areas.¹²¹ A simplified but typical data flow of a feed-forward ANN is shown in Fig. 9(a). In this ANN, the input data move in a forward direction. A series of data nodes (artificial neurons) are integrated to form the layer of input. Within the ANNs, the input signal is passed through one or more hidden layers. At the end of this network, the output layer generates the predicted results. Different from the current von Neumann computer that performs tasks by the pre-design of the program, the ANNs can learn to run a task through a group of training datasets. For example, one of the typical learning processes is the supervised learning method by updating weights with the backpropagation errors between known target values and the output values.¹²² Choosing appropriate hyper parameters in a neural network has a vital role in the training of ANNs models. The final step is to evaluate the performance of the model by calculating the

error in the prediction of outputs. The smaller difference between errors in training data and testing data indicates the more superior generalization of the model.

5.1 ANNs-Enabled Optimization of DLW

Developing an accurate ANNs algorithm for DLW to describe the relationship between output and input variables in the DLW process is of great importance to tackling challenges induced by the dynamic nature of DLW.^{123,124} As is discussed in Sec. 3, the most influential parameters associated with DLW can be generalized into geometrical parameters (fabrication scheme), material parameters (choice of the photoresists), and system parameters (laser setup, etc.). Based on the results from theoretical and experimental data, the performance of DLW can be enhanced significantly by choosing these parameters adequately. The effective parameters in DLW are shown in Fig. 9(b).

For instance, to improve the laser focusing efficiency and quality, ANNs enabled adaptive optics technology was used for fast focusing of a Gaussian beam with wave-front aberration correction and recovery of near-diffraction-limited focal spots. The ANN was trained to determine low-order aberrations from distorted point spread function images detected using a complementary metal-oxide semiconductor (CMOS) camera with Zernike mode coefficients [shown in Fig. 10(a)].^{125,127} Similarly, various ANNs have been applied to laser processing techniques to optimize the parameters. Taguchi and his group created a novel ANNs-based technique to effectively optimize the laser welding parameter,^{126,128} and the combination of these two methods can also obtain good, optimized fabrication results [shown in Fig. 10(b)]. Taguchi's method is widely used in optimizing the laser processing parameters; this approach can reduce the time and cost for the experimental investigations.¹²⁹ To improve the depth-width ratio of the laser welding, Ai et al.¹³⁰ applied the Taguchi method to optimize three welding parameters, i.e., the laser power, welding speed, and focal position. Results showed the reliability and effectiveness of the proposed method. In addition, ANNs for path optimization can improve the fabrication efficiency (in terms of time and cost), while the traditional fabrication schemes of DLW are based on line-by-line scanning techniques and will cost an unachievable amount of time.¹³¹

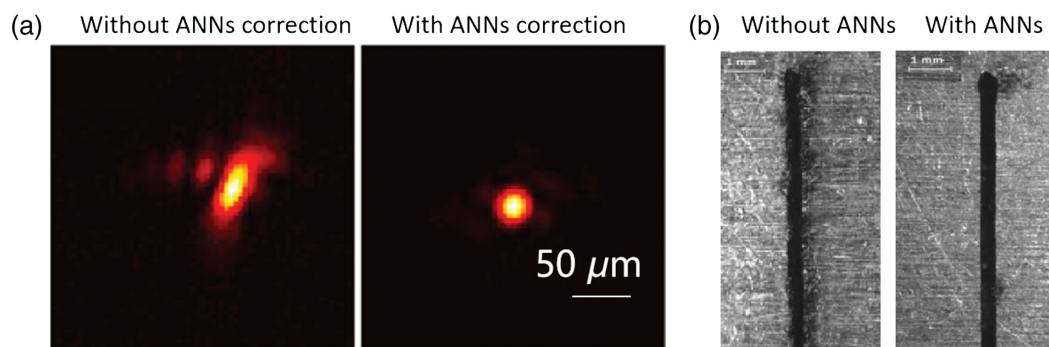


Fig. 10 ANNs-based adaptive optics technology for laser focusing optimization. (a) ANNs-based adaptive optics techniques enable the aberration correction of Gaussian-shaped laser beams.¹²⁵ (b) Experimental results of Kerf acquired without and with optimized focusing parameters.¹²⁶

5.2 ANNs-Enabled Inverse Design of Biomimetic Neuron Interfaces

Recent research in ANNs has been able to help scientists reveal the brain's structure,¹³² where the 3D wiring diagram of neurons in the animal brain can be automatically distinguished by CNNs. These structural data of BNNs can be inversely translated into novel neuron models to create BNIs based on the principles from biomimicry.

On the other hand, ANNs can also contribute to the design of complex biomimetic interfaces and biomimetic geometry design¹³³ where the geometry of biomimetic interfaces can be mathematically calculated with an interactive ANNs algorithmic description. Such methods have been widely used in computer chip design to solve the high dimensional connection and energy efficiency (power distribution/heat dissipation) problems.¹³⁴ Functional BNIs based on nanophotonics can be inverse designed and incorporated using ANNs. Such inverse design methods based on ANNs can improve the performance of a waveguide-based multiplexer and de-coupler.⁴¹

To date, even though few studies have been done on the direct integration of ANNs and DLW, the possible concept of ANNs implementation in 3D large-scale additive printing has been demonstrated to fix the fabrication failure without interruption of the 3D printing processing and become a revolutionary field in health care.¹³⁵ Therefore, the integration of DLW and ANNs for BNIs would have great potential in the next generation of neural tissue engineering and functional ANNs applications.

6 Conclusion and Outlook

This article reviews the fast developing field of 3D direct laser writing of biomimetic neuron interfaces. It is demonstrated that 3D DLW represents a powerful technique to fabricate 3D BNIs for neuron tissue engineering and ANNs. Indeed, 3D BNIs have proven to be a better ensemble of BNNs compared with the currently popular 2D systems.¹³⁶ Although this field is witnessing a transition from simple to architecturally complex structures, large-scale BNIs could not be facilely achieved using current 3D DLW due to the low fabrication speed and poor quality control.

To fully achieve the scale-up and efficient fabrication of BNIs, the integration of ANNs algorithms with DLW is highly necessary so that the computational cost, qualification cost, and data acquisition/processing cost can be dramatically reduced.^{137,138} In addition, the further optimization of photoresist materials in DLW is also necessary. This includes but is not limited to the development of water-soluble PIs with high TPA cross sections,¹³⁹ development of new composite materials, such as conductive photopolymers and photonic photoresists,^{140,141} so that the fabricated 3D BNIs can be applied with two-photon holography optogenetics,^{142,143} where the functionality of the neurons can be excited and visualized in real time. Along with the ongoing research progress in DLW-enabled quantum dots,¹⁴⁴ artificial memristors,¹⁴⁵ and biomimetic synapses,¹⁴⁶ DLW could also enable the realization of BNIs for innovative ANNs.

Acknowledgments

We would like to acknowledge the support from the Science and Technology Commission of Shanghai Municipality (Grant No. 21DZ1100500), the Shanghai Municipal Science and Technology Major Project, the Shanghai Frontiers Science

Center Program (2021-2025 No. 20), the Zhangjiang National Innovation Demonstration Zone (Grant No. ZJ2019-ZD-005), the National Key Research and Development Program of China (Grant No. 2021YFB2802000), and the National Natural Science Foundation of China (Grant No. 61975123).

References

1. A. D. Maynard, "Could we 3D print an artificial mind?" *Nat. Nanotechnol.* **9**(12), 955–956 (2014).
2. Q. Zhang et al., "Artificial neural networks enabled by nanophotonics," *Light Sci. Appl.* **8**(3), 42 (2019).
3. S. Lamon et al., "Nanophotonics-enabled optical data storage in the age of machine learning," *APL Photonics* **6**(11), 110902 (2021).
4. O. Sporns et al., "The human connectome: a structural description of the human brain," *PLoS Comput. Biol.* **1**(4), e42 (2005).
5. O. Sporn, *Discovering the Human Connectome*, MIT Press, Cambridge, Massachusetts (2012).
6. J. M. Benyus, *Biomimicry: Innovation Inspired by Nature*, p. 320, Morrow, New York (1997).
7. E. Stratakis et al., "Laser engineering of biomimetic surfaces," *Mater. Sci. Eng.: R: Rep.* **141**, 100562 (2020).
8. F. U. Rehman et al., "Blood-brain barrier amenable gold nanoparticles biofabrication in aged cell culture medium," *Mater. Today Bio.* **8**, 100072 (2020).
9. E. Stratakis, H. Jeon, and S. Koo, "Structures for biomimetic, fluidic, and biological applications," *MRS Bull.* **41**(12), 993–1001 (2016).
10. T. R. Insel et al., "The NIH brain initiative," *Science* **340**(6133), 687–688 (2013).
11. H. Markram, "The human brain project," *Sci. Am.* **306**(6), 50–55 (2012).
12. S. G. Mason et al., "A comprehensive survey of brain interface technology designs," *Ann. Biomed. Eng.* **35**(2), 137–169 (2007).
13. M. M. Poo et al., "China brain project: basic neuroscience, brain diseases, and brain-inspired computing," *Neuron* **92**(3), 591–596 (2016).
14. H. Okano et al., "Brain/MINDS: brain-mapping project in Japan," *Philos. Trans. R. Soc. B: Biol. Sci.* **370**(1668), 20140310 (2015).
15. Australian Brain Alliance Steering Committee, "Australian brain alliance," *Neuron* **92**(3), 597–600 (2016).
16. J. A. Bierer et al., "Probing the electrode-neuron interface with focused cochlear implant stimulation," *Trends Amplif. J.* **14**(2), 84–95 (2010).
17. J. Abbott et al., "A nanoelectrode array for obtaining intracellular recordings from thousands of connected neurons," *Nat. Biomed. Eng.* **4**(2), 232–241 (2020).
18. A. Stett et al., "Two-way silicon-neuron interface by electrical induction," *Phys. Rev. E* **55**(2), 1779–1782 (1997).
19. P. Fromherz, "The neuron-semiconductor interface," in *Bioelectronics: From Theory to Applications*, pp. 339–394, Wiley-VCH Verlag GmbH and Co., KGaA (2005).
20. R. Lozano et al., "3D printing of layered brain-like structures using peptide modified gellan gum substrates," *Biomaterials* **67**, 264–273 (2015).
21. A. A. Gill et al., "Towards the fabrication of artificial 3D micro-devices for neural cell networks," *Biomed. Microdevices* **17**(2), 27 (2015).
22. M. C. LaPlaca et al., *Methods in Bioengineering: 3D Tissue Engineering*, Artech House, Houston, Texas (2010).
23. A. K. Vogt et al., "Synaptic plasticity in micropatterned neuronal networks," *Biomaterials* **26**(15), 2549–2557 (2005).
24. M. Jungblut et al., "Triangular neuronal networks on micro-electrode arrays: an approach to improve the properties of low-density networks for extracellular recording," *Biomed. Microdevices* **11**(6), 1269 (2009).

25. J. M. Corey et al., "Compliance of hippocampal neurons to patterned substrate networks," *J. Neurosci.* **30**(2), 300–307 (1991).
26. H. Onoe et al., "Microfabricated mobile microplates for handling single adherent cells," *J. Micromech. Microeng.* **18**(9), 095003 (2008).
27. J. Koffler et al., "Biomimetic 3D-printed scaffolds for spinal cord injury repair," *Nat. Med.* **25**(2), 263–269 (2019).
28. T. Mammoto et al., "Mechanical control of tissue and organ development," *Development* **137**(9), 1407–1420 (2010).
29. A. Selimis et al., "Direct laser writing: principles and materials for scaffold 3D printing," *Microelectron. Eng.* **132**, 83–89 (2015).
30. A. M. Taylor et al., "A microfluidic culture platform for CNS axonal injury, regeneration and transport," *Nat. Methods* **2**(8), 599 (2005).
31. M. Merz et al., "Silicon chip interfaced with a geometrically defined net of snail neurons," *Adv. Funct. Mater.* **15**(5), 739–744 (2005).
32. P. Gruber et al., *Biomimetics—Materials, Structures and Processes: Examples, Ideas and Case Studies*, Springer Science & Business Media (2011).
33. D. B. Chklovskii, "Synaptic connectivity and neuronal morphology: two sides of the same coin," *Neuron* **43**(5), 609–617 (2004).
34. J. M. J. Murre and D. P. Sturdy, "The connectivity of the brain: multi-level quantitative analysis," *Biol. Cybern.* **73**(6), 529–545 (1995).
35. W. Liet et al., "NeuroArray: a universal interface for patterning and interrogating neural circuitry with single cell resolution," *Sci. Rep.* **4**(1), 4784 (2014).
36. T. J. Hinton et al., "Three-dimensional printing of complex biological structures by freeform reversible embedding of suspended hydrogels," *Sci. Adv.* **1**(9), e1500758 (2015).
37. S. Kawata et al., "Finer features for functional microdevices," *Nature* **412**(6848), 697–698 (2001).
38. Z. Gan et al., "Three-dimensional deep sub-diffraction optical beam lithography with 9 nm feature size," *Nat. Commun.* **4**(1), 2061 (2013).
39. M. T. Raimondi et al., "Two-photon laser polymerization: from fundamentals to biomedical application in tissue engineering and regenerative medicine," *J. Appl. Biomater. Funct. Mater.* **10**(1), 56–66 (2012).
40. M. I. Jordan et al., "Machine learning: trends, perspectives, and prospects," *Science* **349**(6245), 255–260 (2015).
41. S. Molesky et al., "Inverse design in nanophotonics," *Nat. Photonics* **12**(11), 659–670 (2018).
42. D. Melati et al., "Mapping the global design space of nanophotonic components using machine learning pattern recognition," *Nat. Commun.* **10**(1), 4775 (2019).
43. P. R. Wiecha et al., "Deep learning meets nanophotonics: a generalized accurate predictor for near fields and far fields of arbitrary 3D nanostructures," *Nano Lett.* **20**(1), 329–338 (2019).
44. A. Accardo et al., "Two-photon lithography and microscopy of 3D hydrogel scaffolds for neuronal cell growth," *Biomed. Phys. Eng. Express* **4**(2), 027009 (2018).
45. G. Jensen et al., "3D tissue engineering, an emerging technique for pharmaceutical research," *Acta Pharm. Sin. B* **8**(5), 756–766 (2018).
46. L. B. Pan et al., "Large extracellular spikes recordable from axons in microtunnels," *IEEE Trans. Neural Syst. Rehabil. Eng.* **22**(3), 453–459 (2013).
47. K. Taniguchi et al., "Lumen formation is an intrinsic property of isolated human pluripotent stem cells," *Stem Cell Rep.* **5**(6), 954–962 (2015).
48. D. N. Heo et al., "Multifunctional hydrogel coatings on the surface of neural cuff electrode for improving electrode-nerve tissue interfaces," *Acta Biomater.* **39**, 25–33 (2016).
49. V. Kuzmenko et al., "Tailor-made conductive inks from cellulose nanofibrils for 3D printing of neural guidelines," *Carbohydr. Polym.* **189**, 22–30 (2018).
50. V. Melissinaki et al., "Direct laser writing of 3D scaffolds for neural tissue engineering applications," *Biofabrication* **3**(4), 045005 (2011).
51. M. Y. Laura et al., "Promoting neuron adhesion and growth," *Mater. Today* **11**(5), 36–43 (2008).
52. D. R. Kipke et al., "Silicon-substrate intracortical microelectrode arrays for long-term recording of neuronal spike activity in cerebral cortex," *IEEE Trans. Neural Syst. Rehabil. Eng.* **11**(2), 151–155 (2003).
53. G. Shahaf et al., "Learning in networks of cortical neurons," *J. Neurosci.* **21**(22), 8782–8788 (2001).
54. O. Feinerman et al., "Reliable neuronal logic devices from patterned hippocampal cultures," *Nat. Phys.* **4**(12), 967–973 (2008).
55. S. Fu et al., "3D printing of layered mesoporous bioactive glass/sodium alginate-sodium alginate scaffolds with controllable dual-drug release behaviors," *Biomed. Mater.* **14**(6), 065011 (2019).
56. J. Xing et al., "Improving spatial resolution of two-photon microfabrication by using photoinitiator with high initiating efficiency," *Appl. Phys. Lett.* **90**(13), 131106 (2017).
57. C. Wyart et al., "Constrained synaptic connectivity in functional mammalian neuronal networks grown on patterned surfaces," *J. Neurosci. Methods* **117**(2), 123–131 (2002).
58. P. Tayalia et al., "3D cell-migration studies using two-photon engineered polymer scaffolds," *Adv. Mater.* **20**(23), 4494–4498 (2008).
59. S. Turunen et al., "Direct laser writing of microstructures for the growth guidance of human pluripotent stem cell derived neuronal cells," *Opt. Lasers Eng.* **55**, 197–204 (2014).
60. S. Turunen et al., "Direct laser writing of tubular microtowers for 3D culture of human pluripotent stem cell-derived neuronal cells," *ACS Appl. Mater. Interfaces* **9**(31), 25717–25730 (2017).
61. F. Klein et al., "Elastic fully three-dimensional microstructure scaffolds for cell force measurements," *Adv. Mater.* **22**(8), 868–871 (2010).
62. S. K. Seidlits et al., "High-resolution patterning of hydrogels in three dimensions using direct-write photofabrication for cell guidance," *Adv. Funct. Mater.* **19**(22), 3543–3551 (2009).
63. J. Torgersen et al., Photo-sensitive hydrogels for three-dimensional laser microfabrication in the presence of whole organisms, *J. Biomed. Opt.* **17**(10), 105008 (2012).
64. J. Moughames et al., "Three-dimensional waveguide interconnects for scalable integration of photonic neural networks," *Optica* **7**(6), 640–646 (2020).
65. M. D. Tang-Schomer et al., "Bioengineered functional brain-like cortical tissue," *Proc. Natl. Acad. Sci. U. S. A.* **111**(38), 13811–13816 (2014).
66. M. G. Tupone et al., "A state-of-the-art of functional scaffolds for 3D nervous tissue regeneration," *Front. Bioeng. Biotechnol.* **9**, 639765 (2021).
67. H. Yu et al., "Three-dimensional direct laser writing of biomimetic neuron structures," *Opt. Express* **26**(24), 32111–32117 (2018).
68. X. Fang et al., "Orbital angular momentum holography for high-security encryption," *Nat. Photonics* **14**(2), 102–108.
69. A. Accardo et al., "Multiphoton direct laser writing and 3D imaging of polymeric freestanding architectures for cell colonization," *Small* **13**(27), 1700621 (2017).
70. J. Fischer et al., "Three-dimensional optical laser lithography beyond the diffraction limit," *Laser Photonics Rev.* **7**(1), 22–44 (2013).
71. M. Malinauskas et al., "Ultrafast laser nanostructuring of photopolymers: a decade of advances," *Phys. Rep.* **533**(1), 1–31 (2013).
72. P. V. Ferreras et al., "Development of functional sub-100 nm structures with 3D two-photon polymerization technique and optical methods for characterization," *J. Laser Appl.* **24**(4), 042004 (2012).

73. M. Thiel et al., "Direct laser writing of three-dimensional sub-micron structures using a continuous wave laser at 532 nm," *Appl. Phys. Lett.* **97**(22), 221102 (2010).
74. V. Hahnet al., "Two-step absorption instead of two-photon absorption in 3D nanoprinting," *Nat. Photonics* **15**(12), 932–938 (2021).
75. Y. Cao et al., "High-photosensitive resin for super-resolution direct-laser-writing based on photoinhibited polymerization," *Opt. Express* **19**(20), 19486–19494 (2011).
76. J. T. Fourkas and S. P. John, "2-Colour photolithography," *Phys. Chem. Chem. Phys.* **16**(19), 8731–8750 (2014).
77. H. Yu et al., "Three-dimensional direct laser writing of PEGda hydrogel microstructures with low threshold power using a green laser beam," *Light: Adv. Manuf.* **9**(1), 1 (2021).
78. S. Wong et al., "Direct laser writing of three-dimensional photonic crystals with a complete photonic bandgap in chalcogenide glasses," *Adv. Mater.* **18**(3), 265–269 (2006).
79. Z. Ganet al., "Biomimetic gyroid nanostructures exceeding their natural origins," *Sci. Adv.* **2**(5), e1600084 (2016).
80. B. P. Cumming et al., "Simultaneous compensation for aberration and axial elongation in three-dimensional laser nanofabrication by a high numerical-aperture objective," *Opt. Express* **21**(16), 19135–19141 (2013).
81. A. Jesacher et al., "Adaptive optics for direct laser writing with plasma emission aberration sensing," *Opt. Express* **18**(2), 656–661 (2010).
82. M. D. Turner et al., "Miniature chiral beamsplitter based on gyroid photonic crystals," *Nat. Photonics* **7**(10), 801–805 (2013).
83. M. Göppert-Mayer, "Elementary processes with two quantum transitions," *Ann. Phys.* **18**(7–8), 466–479 (2009).
84. M. H. Olsen et al., "In-chip fabrication of free-form 3D constructs for directed cell migration analysis," *Lab Chip* **13**(24), 4800–4809 (2013).
85. J. Mačiulaitis et al., "Preclinical study of SZ2080 material 3D microstructured scaffolds for cartilage tissue engineering made by femtosecond direct laser writing lithography," *Biofabrication* **7**(1), 015015 (2015).
86. S. Fan et al., "Guiding the patterned growth of neuronal axons and dendrites using anisotropic micropillar scaffolds," *Adv. Healthcare Mater.* **10**(12), 2100094 (2021).
87. J. Wu et al., "Biomimetic nanofibrous scaffolds for neural tissue engineering and drug development," *Drug Discov. Today* **22**(9), 1375–1384 (2017).
88. W. Zhu et al., "3D printing of functional biomaterials for tissue engineering," *Curr. Opin. Biotechnol.* **40**, 103–112 (2016).
89. S. Maruo et al., "Three-dimensional microfabrication with two-photon-absorbed photopolymerization," *Opt. Lett.* **22**(2), 132–134 (1997).
90. D. K. Cullen et al., "Neural tissue engineering and biohybridized microsystems for neurobiological investigation *in vitro* (part 1)," *Crit. Rev. Bioeng.* **39**, 201–240 (2011).
91. G. Márton et al., "The neural tissue around SU-8 implants: a quantitative *in vivo* biocompatibility study," *Mater. Sci. Eng.* **112**, 110870 (2020).
92. S. H. Cho et al., "Biocompatible SU-8-based microprobes for recording neural spike signals from re-generated peripheral nerve fibers," *IEEE Sens. J.* **8**(11), 1830–1836 (2008).
93. M. Farsari et al., "Multiphoton polymerization of hybrid materials," *J. Opt.* **12**(12), 124001 (2010).
94. M. Popall et al., "ORMOCERs as inorganic–organic electrolytes for new solid state lithium batteries and supercapacitors," *Electrochim. Acta* **43**(10), 1155–1161 (1998).
95. K. Terzaki et al., "3D conducting nanostructures fabricated using direct laser writing," *Opt. Mater.* **1**(4), 586–597 (2011).
96. P. S. Timashev et al., "3D *in vitro* platform produced by two-photon polymerization for the analysis of neural network formation and function," *Biomed. Phys. Eng. Express* **2**(3), 035001 (2016).
97. M. T. Raimondi et al., "Three-dimensional structural niches engineered via two-photon laser polymerization promote stem cell homing," *Acta Biomater.* **9**(1), 4579–4584 (2013).
98. A. Ovsianikov et al., "Ultra-low shrinkage hybrid photosensitive material for two-photon polymerization microfabrication," *ACS Nano* **2**(11), 2257–2262 (2008).
99. S. Psycharakis et al., "Tailor-made three-dimensional hybrid scaffolds for cell cultures," *Biomed. Mater.* **6**(4), 045008 (2011).
100. T. Haddad et al., "Fabrication and surface modification of poly lactic acid (PLA) scaffolds with epidermal growth factor for neural tissue engineering," *Biomatter* **6**(1), e1231276 (2016).
101. J. Torgersen et al., "Hydrogels for two-photon polymerization: a toolbox for mimicking the extracellular matrix," *Adv. Funct. Mater.* **23**(36), 4542–4554 (2013).
102. G. D. Nicodemus and S. J. Bryant, "Cell encapsulation in biodegradable hydrogels for tissue engineering applications," *Tissue Eng. Part B: Rev.* **14**(2), 149–165 (2008).
103. O. Kufelt et al., "Hyaluronic acid based materials for scaffolding via two-photon polymerization," *Biomacromolecules* **15**(2), 650–659 (2014).
104. T. Y. Cheng et al., "Neural stem cells encapsulated in a functionalized self-assembling peptide hydrogel for brain tissue engineering," *Biomaterials* **34**(8), 2005–2016 (2013).
105. Y. Yu et al., "Bioinspired helical microfibers from microfluidics," *Adv. Mater.* **29**(18), 1605765 (2017).
106. F. Fu et al., "Bio-inspired self-healing structural color hydrogel," *Proc. Natl. Acad. Sci. U. S. A.* **114**(23), 5900–5905 (2017).
107. Z. Xie et al., "Self-assembled coffee-ring colloidal crystals for structurally colored contact lenses," *Small* **11**(8), 926–930 (2015).
108. H. A. Houck et al., "Shining light on poly (ethylene glycol): from polymer modification to 3D laser printing of water erasable microstructures," *Adv. Mater.* **32**(34), 2003060 (2021).
109. T. Weiß et al., "Two-photon polymerization of biocompatible photopolymers for microstructured 3D biointerfaces," *Adv. Eng. Mater.* **13**(9), B264–B273 (2011).
110. A. Ovsianikov et al., "Three-dimensional laser micro- and nanostructuring of acrylated poly(ethylene glycol) materials and evaluation of their cytotoxicity for tissue engineering applications," *Acta Biomater.* **7**(3), 967–974 (2011).
111. J. D. Pitts et al., "New photoactivators for multiphoton excited three-dimensional submicron cross-linking of proteins: bovine serum albumin and type 1 collagen," *Photochem. Photobiol.* **76**(2), 135–144 (2002).
112. L. P. Cunningham et al., "Freeform multiphoton excited microfabrication for biological applications using a rapid prototyping CAD-based approach," *Opt. Express* **14**(19), 8613–8621 (2006).
113. S. Basu et al., "Multiphoton excited fabrication of collagen matrixes cross-linked by a modified benzophenone dimer: bioactivity and enzymatic degradation," *Biomacromolecules* **6**(3), 1465–1474 (2005).
114. X. H. Qin et al., "Three-dimensional microfabrication of protein hydrogels via two-photon-excited thiol-vinyl ester photopolymerization," *J. Polym. Sci. A Polym. Chem.* **51**(22), 4799–4810 (2013).
115. J. Shamir et al., "Massive holographic interconnection networks and their limitations," *Appl. Opt.* **28**(2), 311 (1989).
116. H. Yu et al., "Neuron-inspired Steiner tree networks for 3D low-density metastructures," *Adv. Sci.* **8**(19), 2100141 (2021).
117. Z. S. Hou et al., "UV–NIR femtosecond laser hybrid lithography for efficient printing of complex on-chip waveguides," *Opt. Lett.* **45**(7), 1862–1865 (2020).
118. H. Ding et al., "3D computer-aided nanoprinting for solid-state nanopores," *Nanoscale Horiz.* **3**(3), 312–316 (2018).
119. K. Eichler et al., "The complete connectome of a learning and memory centre in an insect brain," *Nature* **548**(7666), 175–182 (2017).

120. H. Yu et al., "Deep-learning-aided three-dimensional direct laser writing of the complete connectome of mushroom body from an insect brain," in *Eur. Quantum Electron. Conf.*, Optical Society of America, p. jsi_p_1 (2019).
121. B. H. Li et al., "Applications of artificial intelligence in intelligent manufacturing: a review," *Front. Inf. Technol. Electron. Eng.* **18**(1), 86–96 (2017).
122. G. Hinton, "Mental simulation," *Nature* **347**(6294), 627–628 (1990).
123. J. B. Mueller et al., "Polymerization kinetics in three-dimensional direct laser writing," *Adv. Mater.* **26**(38), 6566–6571 (2014).
124. A. Li et al., "Micro-optical sectioning tomography to obtain a high-resolution Atlas of the mouse brain," *Science* **330**(6009), 1404–1408 (2010).
125. Y. Jin et al., "Machine learning guided rapid focusing with sensor-less aberration corrections," *Opt. Express* **26**(23), 30162–30171 (2018).
126. S. L. Campanelli et al., "An artificial neural network approach for the control of the laser milling process," *Int. J. Adv. Manuf. Technol.* **66**(9–12), 1777–1784 (2013).
127. B. P. Cumming and M. Gu, "Direct determination of aberration functions in microscopy by an artificial neural network," *Opt. Express* **28**(10), 14511–14521 (2020).
128. S. Pal et al., "Artificial neural network modeling of weld joint strength prediction of a pulsed metal inert gas welding process using arc signals," *J. Mater. Process Technol.* **202**(1–3), 464–474 (2008).
129. D. S. Badkar et al., "Parameter optimization of laser transformation hardening by using Taguchi method and utility concept," *Int. J. Adv. Manuf. Technol.* **52**(9), 1067–1077 (2011).
130. Y. Ai et al., "Parameters optimization and objective trend analysis for fiber laser keyhole welding based on Taguchi-FEA," *Int. J. Adv. Manuf. Technol.* **90**(5), 1419–1432 (2017).
131. S. Theodoridis, *Machine Learning: A Bayesian and Optimization Perspective*, Academic Press, Salt Lake City, Utah (2015).
132. M. Januszewski et al., "High-precision automated reconstruction of neurons with flood-filling networks," *Nat. Methods* **15**(8), 605–610 (2018).
133. T. J. Kowalski, *An Artificial Intelligence Approach to VLSI Design*, United States (1985).
134. A. Mirhoseini et al., "A graph placement methodology for fast chip design," *Nature* **594**(7862), 207–212 (2021).
135. A. Banerjee et al., "Artificial intelligence in 3D printing: a revolution in health care," in *Emerging Applications of 3D Printing During COVID 19 Pandemic*, pp. 57–79, Springer, Singapore (2022).
136. R. Vidu et al., "Nanostructures: a platform for brain repair and augmentation," *Front. Syst. Neurosci.* **8**, 91 (2014).
137. U. Delli et al., "Automated process monitoring in 3D printing using supervised machine learning," *Procedia Manuf.* **26**, 865–870 (2018).
138. T. Wuest et al., "An approach to monitoring quality in manufacturing using supervised machine learning on product state data," *J. Intell. Manuf.* **25**(5), 1167–1180 (2014).
139. X. Gou et al., "Mechanical property of PEG hydrogel and the 3D red blood cell microstructures fabricated by two-photon polymerization," *Appl. Surf. Sci.* **416**, 273–280 (2017).
140. S. Jiguet et al., "Conductive SU8 photoresist for microfabrication," *Adv. Funct. Mater.* **15**(9), 1511–1516 (2005).
141. M. Del Pozo et al., "Direct laser writing of four-dimensional structural color microactuators using a photonic photoresist," *ACS Nano* **14**(8), 9832–9839 (2020).
142. J. H. Marshel et al., "Cortical layer-specific critical dynamics triggering perception," *Science* **365**(6453), eaaw5202 (2019).
143. H. Xie et al., "In vivo imaging of immediate early gene expression reveals layer-specific memory traces in the mammalian brain," *Proc. Natl. Acad. Sci. U. S. A.* **111**(7), 2788–2793 (2014).
144. M. Barbiero et al., "Spin-manipulated nanoscopy for single nitrogen-vacancy center localizations in nanodiamonds," *Light Sci. Appl.* **6**(11), e17085 (2017).
145. R. S. Williams, "How we found the missing memristor," *IEEE Spectr.* **45**(12), 28–35 (2008).
146. M. S. Hasan et al., "Biomimetic, soft-material synapse for neuro-morphic computing: from device to network," in *IEEE 13th Dallas Circuits and Syst. Conf.*, IEEE, pp. 1–6 (2018).

Haoyi Yu received his MSc degree from Nankai University in 2015 and his PhD from RMIT University in Australia in 2019. Currently, he is appointed as a research fellow at the Centre for Artificial-Intelligence Nanophotonics (CAIN), and Institute of Photonic Chips, University of Shanghai for Science and Technology. His research interests include nanophotonics, artificial neural networks, and biophotonics. He has published more than 10 research works in such journals as *Advanced Science*, *Light: Science and Applications*, and *Optics Express*.

Qiming Zhang received his PhD in optical science from Fudan University in 2011. He had been a senior researcher of RMIT in Australia before he joined USST in 2019. He has published more than 30 papers in such journals as *Science*, *Nature Photonics*, *Nature Communications*, *Nature Review Materials*, and *Optics Letters*. His research interests include center on artificial intelligence nanophotonics device, optical information storage, and femtosecond optical processing.

Xi Chen received his PhD from Queensland University of Technology in 2010, and joined University of Shanghai for Science and Technology in 2019. His research fields are artificial intelligence materials, laser fabrication, and supercapacitors. He has published SCI papers in international journals such as *Advanced Materials* and *Nano Letters*.

Haitao Luan received his MSc degree from University of Kassel in 2013 and commenced to Centre for Micro-Photonics (CMP) to pursue a PhD studentship. He received his PhD from RMIT University in 2019 and subsequently was appointed a research fellow at Centre for Artificial-Intelligence Nanophotonics (CAIN) in University of Shanghai for Science and Technology. Currently, he is a research professor and an assistant director (Innovation) of Institute of Photonic Chips (IPC) of USST.

Min Gu is an executive chancellor of the University Council and a distinguished professor of University of Shanghai for Science and Technology. He was a distinguished professor and an associate deputy vice-chancellor at RMIT University and a laureate fellow of the Australian Research Council. He is an elected fellow of the Australian Academy of Science and the Australian Academy of Technological Sciences and Engineering, and foreign fellow of the Chinese Academy of Engineering. He was awarded the Einstein Professorship, the W. H. (Beattie) Steel Medal, the Ian Wark Medal, the Boas Medal, the Victoria Prize for Science and Innovation, the Dennis Gabor Award, and the Emmett N. Leith Medal.